ELSEVIER

Contents lists available at ScienceDirect

Materials Today Electronics

journal homepage: www.elsevier.com/locate/mtelec



Investigation of deep defects and their effects on the properties of NiO/ β -Ga₂O₃ heterojuncion diodes



Abdulaziz Almalki ^{a,b,*}, Labed Madani ^c, Nouredine Sengouga ^d, Sultan Alhassan ^e, Saud Alotaibi ^{a,f}, Amra Alhassni ^{a,g}, Amjad Almunyif ^{a,h}, Jasbinder S. Chauhan ^a, Mohamed Henini ^a, Helder Vinicius Avanço Galeti ⁱ, Yara Galvão Gobato ^j, Marcio Peron Franco de Godoy ^j, Marcelo B. Andrade ^{k,o}, Sérgio Souto ^l, Hong Zhou ^m, Boyan Wang ⁿ, Ming Xiao ⁿ, Yuan Qin ⁿ, Yuhao Zhang ⁿ

- ^a School of Physics and Astronomy, University of Nottingham, Nottingham NG7 2RD, UK
- b Physics Department, Faculty of Science at Taibah University-Yanbu, King Khalid Rd. Al Amoedi, 46423, Yanbu El-Bahr, 51000, Saudi Arabia
- ^c Department of Intelligent Mechatronics Engineering, Sejong University, 209 Neungdong-ro, Gwangjin-gu, Seoul 05006, Republic of Korea
- ^d Laboratory of Semiconducting and Metallic Materials (LMSM), University of Biskra 07000, Algeria
- ^e Physics Department, College of Science, Jouf University, P.O. Box:2014, Sakaka, Saudi Arabia
- ^fPhysics Department, Faculty of Science and Humanities in Ad-Dawadmi, Shaqra University, 11911, Saudi Aribia
- g Physics Department, Al-Baha University, 65931, Al-Makhwah, Saudi Arabia
- h Department of physics, College of sciences, Princess Nourah bint Abdulrahman University (PNU), Riyadh 11671, Saudi Aribia
- i Departamento de Engenharia Elétrica, Universidade Federal de São Carlos (UFSCAR), 13560-905 São Carlos, SP, Brazil
- ^j Departamento de Física, Universidade Federal de São Carlos (UFSCAR), 13560-905 São Carlos, SP, Brazil, Universidade Federal e São Carlos
- ^k São Carlos Institute of Physics, University of São Paulo, PO Box 369, São Carlos, SP 13560-970, Brazil
- Departamento de Ciências Básicas-Faculdade de Zootecnia e Engenharia de Alimentos, Universidade de São Paulo, CEP 13635-900 Pirassununga, SP, Brazil
- m School of Microelectronics, Xidian University, Xi'an, China
- ⁿ Center for Power Electronics Systems, Virginia Polytechnic Institute and State University, Blacksburg, VA, 24060, USA
- ^o Physics Department, Federal University of Ouro Preto, Ouro Preto, MG, 35400-000, Brazil

ARTICLE INFO

Keywords: NiO/ β -Ga₂O₃ heterojunction diodes Defects Deep level transient spectroscopy Photoluminescence Raman Electrical characteristics Modeling

ABSTRACT

In this study, the effect of rapid thermal annealing (RTA) on the electrical and optical properties of NiO/ β-Ga₂O₃ heterojunction diodes was investigated using capacitance-voltage, current-voltage, Deep Level Transient Spectroscopy (DLTS), Laplace DLTS, photoluminescence and micro-Raman spectroscopy techniques, and SILVACO-TCAD numerical simulator. The NiO is designed to be lowly-doped, allowing for the NiO full depletion at zero bias and the study of properties of β -Ga₂O₃ and its interface with NiO. Micro-Raman results revealed good agreement with the theoretical and experimental results reported in the literature. The photoluminescence intensity of the sample after RTA is five times higher than the fresh sample due to a rise in the density of gallium and oxygen vacancies $(V_{Ga} + V_O)$ in the annealed β -Ga₂O₃ samples. The current-voltage characteristics showed that annealed devices exhibited a lower ideality factor at room temperature and higher barrier height compared with fresh samples. The DLTS measurements demonstrated that the number of electrically active traps were different for the two samples. In particular, three and one electron traps were detected in fresh samples and annealed samples, respectively. SILVACO-TCAD was used to understand the distribution of the detected electron E2 trap (E_c-0.15 eV) in the fresh sample and the dominant transport mechanisms. A fairly good agreement between simulation and measurements was achieved considering a surface NiO acceptor density of about 1×10^{19} cm⁻³ and E_2 trap depth into the surface of β- Ga_2O_3 layer of about 0.220 μm and the effect of the most observed E_c -0.75 eV trap level in β-Ga₂O₃. These results unveil comprehensive physics in NiO/β-Ga₂O₃ heterojunction and suggest that RTA is an essential process for realizing high-performance NiO/β -Ga₂O₃ devices.

E-mail address: ppxaa8@nottingham.ac.uk (A. Almalki).

^{*} Corresponding author.

1. Introduction

Ultra-wide bandgap (UWBG) semiconductor gallium oxide (Ga_2O_3) is an excellent candidate for the next generation of power devices, owing to its ultra-wide bandgap of ~4.8 eV, high theoretical breakdown electric field of ~8 MV/cm, and availability of affordable native substrates [1–3]. By taking advantage of these superior physical properties, β -Ga₂O₃ power devices can potentially achieve higher switching frequency, smaller switching losses and higher operation temperatures compared with same current- and breakdown voltage-rated Si, SiC and GaN counterparts [4–6]. To achieve the ultimate limit of β -Ga₂O₃, various device structure innovations have been demonstrated in recent years to advance the device figure-of-merits (FOM) as well as pushing Ga₂O₃ towards circuit applications [7,8]. Among device innovations, different edge termination structures are designed to reduce electric field crowding at the junction periphery. These include mesa, trench, field plate, guard ring, and ion-implanted terminations [9–13].

There are many attempts to develop a stable p-type β -Ga₂O₃ [14– 18] in order to form heterojunctions with the well-established n-type β -Ga₂O₃. However, other p-type materials have been considered to form stable heterojunctions with β -Ga₂O₃ with the aim to achieve high breakdown voltage, lower leakage current and to potentially enhance ruggedness of β -Ga₂O₃ power devices [4,19,20]. Different p-type semiconductors such as Cu_2O , Ir_2O_3 , Ag_2O , CuI and NiO were employed to produce p-n heterojunction with β -Ga₂O₃ [21–25]. Among these p-type materials, NiO is promising for achieving high performance NiO/β-Ga₂O₃ heterojunction diodes (HJDs) due to its easy deposition by sputtering and controllable hole concentration stemming from the nickel vacancy [26]. The NiO/β-Ga₂O₃ system have shown excellent voltage blocking capability. A high breakdown voltage of 1.86 kV and a specific onresistance of 10.6 mΩcm² was reported by using a double-layer NiO [19]. Recently, an improved breakdown voltage of 2.41 kV has been demonstrated based on NiO/β-Ga₂O₃ HJDs with small-angle beveled field plate, achieving a record Baliga's FOM of 5.18 GW cm⁻² [4].

Despite the progress made on NiO/β-Ga₂O₃ HJDs, they still suffer from serious leakage current and premature breakdown [21,27]. These problems may result from defect states in $\beta\text{-}\text{Ga}_2\text{O}_3$ and the NiO/ $\beta\text{-}\text{Ga}_2\text{O}_3$ interface. A deep energy level state below the conduction band (EC) of E_C -0.72 eV was found to be responsible for reverse leakage path in β -Ga₂O₃ Schottky diodes (SBDs) [27]. Even an incomplete ionization of a 110 meV level defect state in unintentionally doped β-Ga₂O₃ may increase the ON-state resistance, decrease the breakdown voltage and cause instabilities of power devices [28]. Hence, it is of vital importance to identify the defect states in β -Ga $_2$ O $_3$ and NiO/ β -Ga $_2$ O $_3$ interface, which is remarkably beneficial for unveiling breakdown and transport mechanisms, as well as improving the reliability of β -Ga₂O₃ power devices. Deep Level Transient Spectroscopy (DLTS), as an efficient and powerful method used for observing and characterizing deep level impurities in semiconductors, was widely used in β -Ga₂O₃. Zhang et al. reported five majority traps spread throughout the Ga₂O₃ energy bandgap characterized using DLTS and optical DLTS (ODLTS) in Ni/Ga2O3 SBDs [29]. A DLTS study of defects in Ga₂O₃:Zr crystals has only shown relatively shallower deep levels [30]. While in β -Ga₂O₃ grown on two differently oriented substrates to realize SBDs, DLTS has identified two deep levels relatively close to the conduction band [31]. Most of the DLTS work are based on β -Ga₂O₃ SBDs. To reveal the defect states of NiO/ β - Ga_2O_3 system, a p^+ -n NiO/β - Ga_2O_3 HJD was fabricated to investigate the majority and minority carrier traps. Energy levels below the conduction (E_C) and above the valence band (E_V) of E_C -(0.75–0.79) eV and E_V + 0.14 eV were identified to be electron and hole traps, respectively

However, the p^+ -n NiO/ β -Ga₂O₃ HJDs used in the aforementioned work has a very shallow depletion into NiO at reverse biases (i.e., unpunched-through NiO). Therefore, it is difficult to exclude the defect states in NiO measured by DLTS. On the other hand, to achieve a high performance NiO/ β -Ga₂O₃ HJD, annealing is an effective way to im-

prove both bulk and heterointerface quality, while the relevant physics has not been fully understood.

To address these gaps, in this work, we designed a NiO/ β -Ga₂O₃ HJDs with a punched-through NiO layer to guarantee that the DLTS signals are detected only from β -Ga₂O₃ bulk and NiO/ β -Ga₂O₃ interface. DLTS measurements were carried out on fresh and annealed HJDs devices. By combining experimental and modeling, this work aims at understanding NiO/ β -Ga₂O₃ HJDs and revealing the dominant conduction mechanisms before and after annealing.

2. Samples details

Fig. 1(a) shows the cross-section schematics of the NiO/ β -Ga₂O₃ HJD. The epitaxial structure consists of a 10-µm thick n-Ga₂O₃ drift layer ($\sim 3 \times 10^{16} \text{ cm}^{-3}$) grown by hydride vapor phase epitaxy (HVPE) on 600 μ m (001) n^+ -Ga₂O₃ substrate. The fabrication process of the NiO/β-Ga₂O₃ HJD was commenced by depositing the back Ohmic contact of Ti/Au (30/150 nm) by electron beam evaporation (EBE), followed by rapid thermal annealing (RTA) at 470 °C in N2 atmosphere for 1 min. 100 nm NiO layer was then sputtered on top of the β-Ga₂O₃ drift layer in pure Ar gas ambient with a flow rate of 60 sccm. This was followed by sputtering a 80 nm thick Ni layer. Finally, the sample was immediately transferred to an electron beam evaporator where a 5 nm/150 nm Ti/Au metal stack was deposited as the anode pad. This was followed by photolithography lift-off process to define circular mesas with an anode diameter of 120 μ m. RTA post-annealing was performed at 225 °C in N2 atmosphere for 15 min to improve Ga2O3/NiO interface quality.

In order to characterize the acceptor concentration (N_A) in NiO, a metal/SiO $_2$ /NiO MOS structure was fabricated, as shown in Fig. 1(b). Highly-doped n-type Si wafer was utilized as the substrate. Ni/Ti/Al metal stack with thickness of 80/20/100 nm was deposited by EBE. NiO layer was sputtered using the same process mentioned above. Then 60 nm SiO $_2$ was deposited by plasma enhanced chemical vapor deposition (PECVD), followed by deposition of Ti/Au (30/150 nm) electrode.

The p-type doping of NiO originates from nickel vacancies [33]. Generally, the N_A value in NiO can be modulated by tuning the Ar/O $_2$ flow ratio during the sputtering process [34]. The lowest N_A value that can be achieved is when there is no O_2 gas flow during the sputtering process. In this work, the NiO was deposited in pure Ar atmosphere with the aim to obtain a very low N_A value which is required to achieve a fully depleted NiO layer.

Fig. 2(a) and (b) show the capacitance-voltage (C-V), $1/C^2$ -V data and fitted $1/C^2$ -V plot of the MOS structures measured at frequency of 1 kHz, before and after the RTA for NiO. The extracted N_A in the NiO before and after annealing is about 8×10^{16} cm⁻³ and 6×10^{16} cm⁻³, respectively. Due to the low N_A and small thickness of NiO, the NiO is totally depleted at zero bias in the NiO/ β -Ga₂O₃ HJD. Therefore, the defect states in NiO can be easily excluded for DLTS analysis.

3. Optical characterization

The role of RTA on Ga_2O_3 was assessed by investigating the optical properties of fresh Ga_2O_3 sample (reference sample) and an annealed Ga_2O_3 sample using photoluminescence and Raman spectroscopy. This RTA condition is the same as the post-annealing for the HJD.

Unpolarized Micro-Raman measurements were performed at room temperature in backscattering geometry. A spectrometer Horiba LabRAM HR Evolution system was used with an 1800 g/mm grating, a 50x objective, laser wavelength 633 nm with a power of 10 mW. The spectral resolution was $\sim 1~\rm cm^{-1}$, and the spectra were measured in the wavenumber range 100 to 900 cm⁻¹ with 100 s accumulation time. Photoluminescence (PL) measurements were carried out at 100–300 K using a Linkam THMS600 cryostat and He–Cd Kimmon Koha laser ($\lambda = 325~\rm nm$) as excitation source with laser power of 30 mW. The spec-

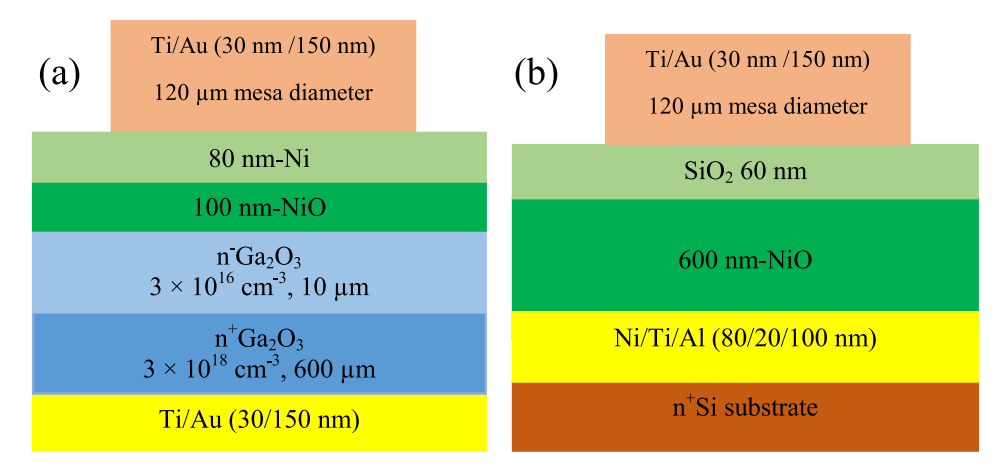


Fig. 1. Schematic cross-section of (a) NiO/ β -Ga₂O₃ HJD, (b) metal/SiO₂/NiO MOS structure for C-V test. (For interpretation of the references to color in this figure legend, the reader is referred to the web version of this article.)

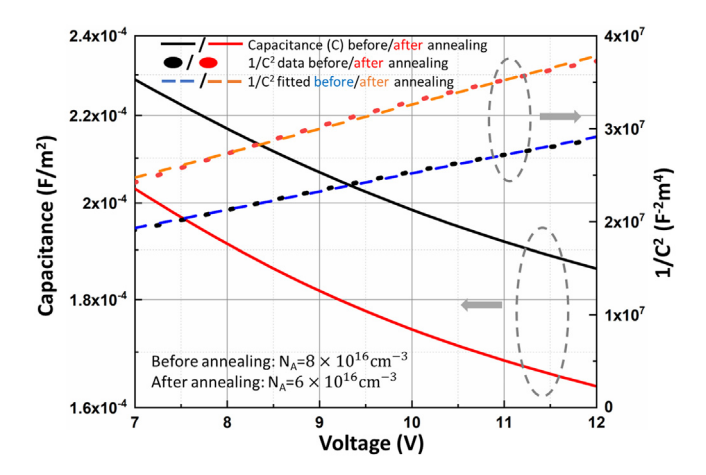


Fig. 2. C-V, $1/C^2$ -V data and fitted $1/C^2$ -V plots of the metal/SiO₂/NiO MOS measured at 1 kHz for NiO before and after annealing. (For interpretation of the references to color in this figure legend, the reader is referred to the web version of this article.)

tra were recorded by an Andor Solis SR500 monochromator using 300 lines/mm diffraction grid and a S-20 photomultiplier.

3.1. Micro-Raman spectroscopy

The Raman spectra of the fresh and annealed Ga_2O_3 samples are similar (Fig. 3). Comparing the spectra, no important frequency shift, linewidth variation, or relative intensity change was observed. Particularly, we observed Raman peaks at 110, 114,144, 169, 200, 320, 346, 416, 475, 629,652, and 766 cm⁻¹. The wavenumbers and width of Raman peaks are in good agreement with the theoretical and experimental results reported in the literature for β -Ga₂O₃ phase, with a monoclinic structure and belongs to the C^3_{2h} space group [35–41]. The nature of the observed peaks depends on the frequency range [35,37,40,41]: for ω < 210 cm⁻¹, they are associated with the low-frequency vibration and translation motion of tetrahedron (GaO₄)—octahedron (Ga₂O₆) chains; for 300 cm⁻¹ < ω < 500 cm⁻¹, they are attributed to the deformation of tetrahedron and octahedron; finally, for ω > 500 cm⁻¹ region is related to the high-frequency stretching and bending of tetrahedra.

The sharp and high-intensity Raman peaks indicate that both β -Ga₂O₃ samples (fresh and annealed) have high crystallinity. From our Raman results, it is also possible to conclude that there is no appreciable change in the crystalline structure after thermal treatment.

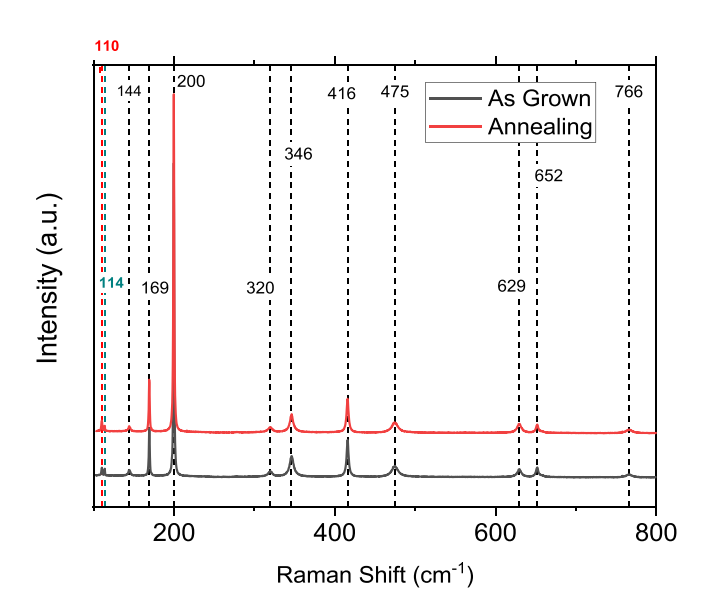


Fig. 3. Raman spectra of fresh and annealed β -Ga₂O₃ samples. (For interpretation of the references to color in this figure legend, the reader is referred to the web version of this article.)

3.2. Photoluminescence spectroscopy

Fig. 4(a) shows typical below bandgap excitation PL spectra of fresh and annealed β -Ga₂O₃ samples at a temperature of 284 K. The broad spectra present a stronger blue band at around 3.0 eV with a weaker green tail at low energies characterized by a band centered at 2.48 eV. It is worth noting that the PL intensity increases about five times after RTA while the PL peak position did not show significant change with thermal annealing. Similar results were observed at lower temperatures (please see Figure S1).

In general, the PL spectrum of β -Ga₂O₃ samples presents several broad bands from UV to the visible region that depend on the doping and different post-treatments [42]. The optical band gap of single-crystal β -Ga₂O₃, usually measured by absorption techniques, is around 4.8 eV for undoped samples [43]. When excited above bandgap, there are four typical PL bands related to β -Ga₂O₃ at around 3.40 eV (UV), 3.10 eV (UV), 2.95 eV (blue), and 2.48 eV (green) [42,43]. The UV band at 3.4 eV (wavelength = 360 nm), which is usually independent of the presence of impurities, decreases fast in intensity with increasing tem-

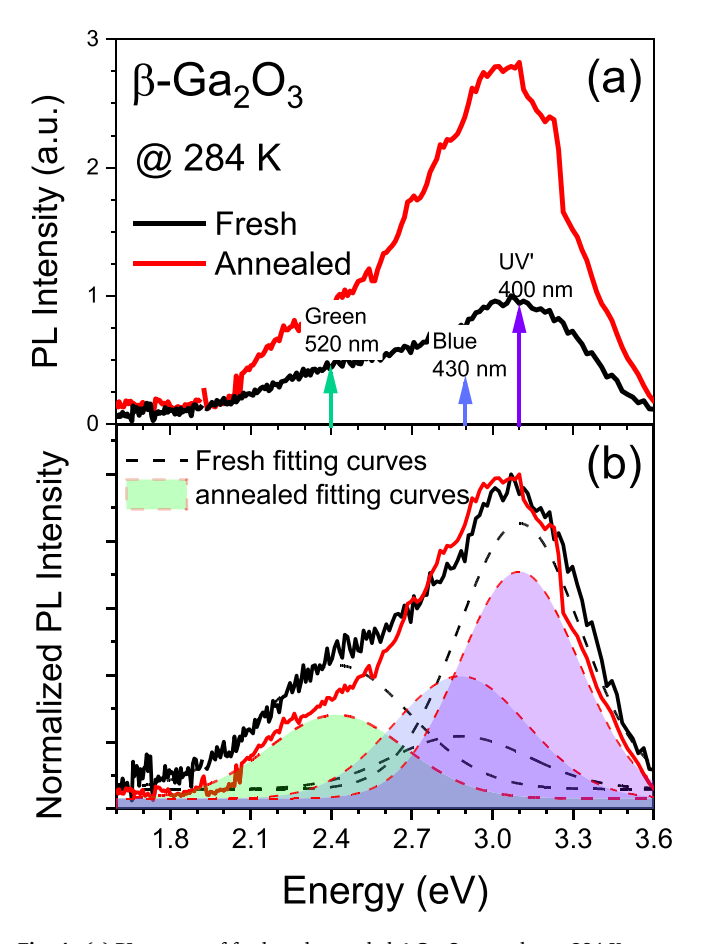


Fig. 4. (a) PL spectra of fresh and annealed β -Ga₂O₃ samples at 284 K present a strong enhancement of intensity after annealing; (b) normalized PL spectra allow the visualization of the role of each defect complex. (For interpretation of the references to color in this figure legend, the reader is referred to the web version of this article.)

perature, and has been attributed early on to electron recombination with a self-trapped hole (STH) [42].

The UV' (3.1 eV or wavelength = 400 nm) and blue PL bands in undoped $\beta\text{-}Ga_2O_3$ samples were previously associated with the recombination of electrons and holes trapped at an acceptor site [36,38]. The type of donors that contribute to the PL are not well understood but they are usually associated with shallow donors [36,38] such as unintentional doping or Ga_i (Ga interstitial). It is important to point out that our samples are doped intentionally using Si atoms, which are shallow donors in $\beta\text{-}Ga_2O_3$ semiconductor materials. The presence of Si increases further the total density of donors in our samples. Gallium vacancy ($V_{\rm Ga}$), divacancy ($V_{\rm Ga}$ + $V_{\rm O}$) and interstitial oxygen ($O_{\rm i}$) have been suggested as acceptor levels [42].

Recent studies have confirmed that transitions involving $V_{Ga} + V_{O}$ acceptor levels could explain the nature of the blue PL band [42]. In addition, deeper electronic levels in the bandgap are responsible for the lower energy emissions [42]. The green PL band at around 520 nm indicates the presence of oxygen-related defects originating from the recombination of electrons with holes trapped by interstitial oxygen (O_i) [42]. The energy positions of these three PL bands are indicated in Fig. 4(a) for clarity.

A deconvolution of the spectra in UV', blue, and green regions by Gaussian curves (dashed lines) shows interesting features. In general, an increase of PL intensity after thermal annealing is observed. Similar enhancements of PL intensity after annealing have been reported previously [44,45]. In addition, the PL spectra in the UV' range exhibit a similar profile as compared to the PL of the as-grown sample as evidenced

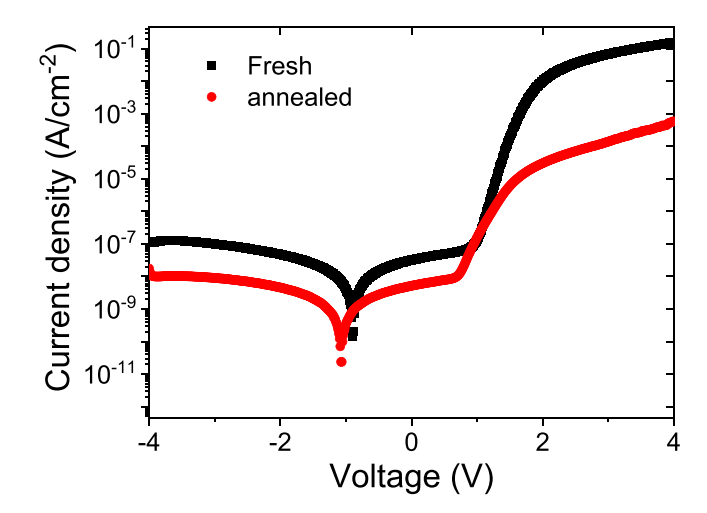


Fig. 5. J-V plots for both fresh and annealed samples. (For interpretation of the references to color in this figure legend, the reader is referred to the web version of this article.)

in the normalized spectra shown in Fig. 4(b). Furthermore, a relative decrease in the lower energy tail is observed for the annealed sample. It is worth noting that the relative intensity of the blue increases after annealing (Fig. 4(b)). In contrast, the relative intensity of the green band decreases. As the blue PL band is associated with the recombination of holes trapped at an acceptor site (acceptors: gallium vacancy $(V_{\rm Ga})$) or the divacancy $(V_{\rm Ga}+V_{\rm O})$ [42], the results would indicate an increase of such VGa vacancies, which is consistent with previous studies in the literature [46,47]. On the other hand, as mentioned above the green PL band, which is correlated to holes trapped at Oi, has shown a decrease of the relative PL intensity after thermal annealing. The observed changes of relative intensity of these bands after thermal annealing and the details on nature of these PL bands in $\beta\text{-Ga}_2\text{O}_3$ is not well understood yet and further studies are needed to shed in more details some light on their origins.

4. Electrical characterization

4.1. Current-voltage and capacitance-voltage characteristics

The current-voltage characteristics (I-V) as a function of temperature (200-340 K with 20 K intervals) were measured on fresh and annealed NiO/β -Ga₂O₃ p-n diodes in order to determine factors such as ideality factor (n), barrier height (\emptyset_B), and series resistance (Rs). Fig. 5 shows a semi-logarithmic current density versus voltage plot (J-V) for fresh and annealed samples at room temperature. Both samples have relatively low leakage current densities. Fig. 5 illustrates that the reverse current density of the annealed samples is lower than that of the fresh samples. The reverse bias current densities at -4 V before annealing and after annealing are 1.17×10^{-7} A/cm⁻² and 1.19×10^{-8} A/cm⁻², respectively. This reduction in reverse current density indicates improved electrical characteristics of the device as a result of the thermal annealing process. A similar behavior has been observed in previous studies on NiO/ β -Ga₂O₃ p-n diodes, where the reverse current was found to rapidly decrease after annealing the device in a nitrogen atmosphere for 3 min at 350 °C [48]. In addition, it is assumed that the lower reverse current observed in the annealed samples is due to a reduction of the number of deep defects or to their concentrations, which act as generation recombination centers [49]. The assumptions will be further investigated using DLTS.

In the heterojunction junction, thermionic current at the band discontinuity is very important. In fact, it is believed that the thermionic emission mechanism is usually predominant in metal-semiconductor

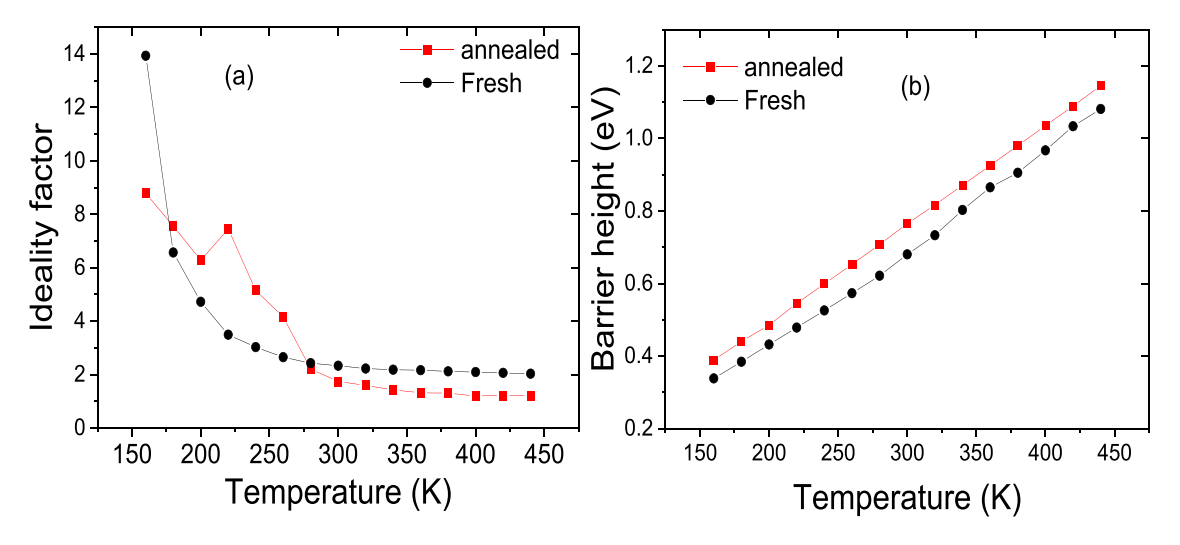


Fig. 6. Temperature dependence of (a) Ideality factor; (b) barrier height, obtained from I-V characteristics for fresh and annealed devices. (For interpretation of the references to color in this figure legend, the reader is referred to the web version of this article.)

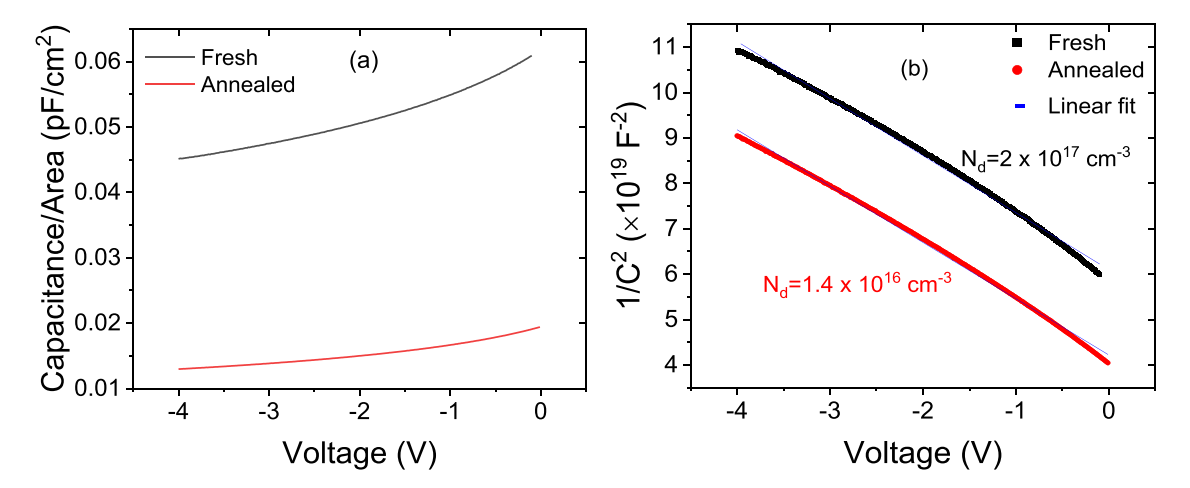


Fig. 7. (a) Plots of C-V characteristics and (b) $1/C^2$ versus V plots for fresh and annealed samples at room temperature (RT). The linear fit to the experimental data is shown in blue. (For interpretation of the references to color in this figure legend, the reader is referred to the web version of this article.)

Schottky contacts which can be regarded as a special case of heterojunctions $\lceil 50 \rceil$.

Current-voltage characteristics of heterogeneous p-n junctions can be described by thermionic emission, as given below [50,51]:

$$I = I_s \left[exp \left(\frac{q(V - IR_s)}{nkT} \right) - 1 \right]$$
 (1)

$$I_s = AA^* T^2 exp\left(\frac{-q\emptyset_B}{kT}\right) \tag{2}$$

where q is the elementary charge, n is the ideality factor, k is Boltzmann's constant, T is the temperature, \emptyset_B is the barrier height, Rs is the series resistance, A is the effective diode area ($A=2.12\times10^{-3}~{\rm cm}^2$ and $8.1\times10^{-3}~{\rm cm}^2$ for fresh and annealed samples, respectively) and A^* is the effective Richardson's constant. Werner's method was used to calculate the diode parameters (n, \emptyset_B and Rs) [52]. The forward I-V characteristics for all samples are used to obtain the series resistance, ideality factors (n), and barrier height (\emptyset_B). These parameters are summarized in Table 1.

The ideality factor in forward bias for fresh and annealed samples, as shown in Table 1, deviates from unity, but it is worth noting that the ideality factor value of annealed sample is much lower than fresh sample. This reduction of ideality factor was reported in NiO/β -Ga₂O₃ p-n diodes after annealing process, demonstrating that thermal treatment

Table 1 Ideality factor (n), barrier height (\emptyset_B) and series resistance (Rs) at room temperature for fresh and annealed devices.

Device	n	\emptyset_B (eV)	Rs (Ω)
Fresh	2.33 ± 0.01	0.68 ± 0.01	0.30 ± 0.01
Annealed	1.74 ± 0.02	0.76 ± 0.01	130 ± 1.01

can significantly enhance the quality of NiO/Ga $_2$ O $_3$ p-n interface and reduce the interface recombination caused by defects [48]. Additionally, if one considers that the ideality factor is around 2 in both samples, then this value is comparable to those obtained for NiO/ β -Ga $_2$ O $_3$ heterojunction diodes reported by Kokubun et al. [22] and Peter et al. [53]. This indicates that the current may be limited by recombination [54,55]. The barrier height values of the annealed and fresh samples were calculated as 0.73 and 0.75 eV at room temperature, respectively. The barrier height value of annealed diodes is lower than fresh samples. This slight reduction of barrier height after annealing could be due to the rapid thermal annealing process. The Rs is dominated by the lightly-doped NiO. Its increase after annealing suggests a reduction of hole concentration.

Fig. 6(a) and (b) show the temperature dependence of the ideality factor and barrier height for fresh and annealed samples over the tem-

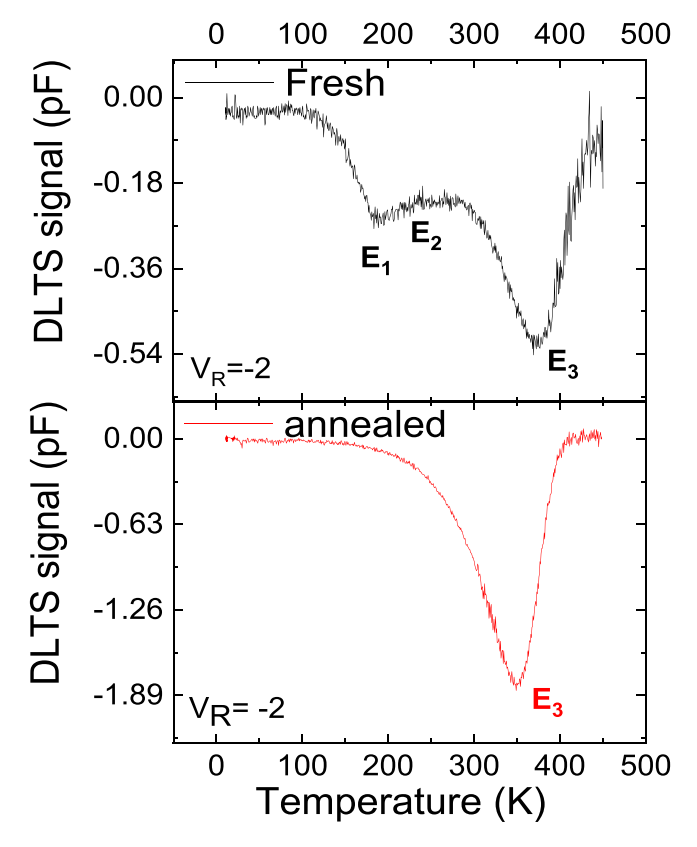


Fig. 8. DLTS spectra for fresh and annealed devices at $V_R = -2$ V. (For interpretation of the references to color in this figure legend, the reader is referred to the web version of this article.)

perature range 100 K to 440 K, respectively. Interestingly, the ideality factor decreased with increasing temperature while the barrier height increased. Similar observations in β -Ga₂O₃ have been reported [56–58]. These changes as a function of temperature are related to inhomogeneous interfaces caused by interfacial traps. According to the inhomogeneity theory, the Schottky barrier height can be considered as a Gaussian distribution, and with increasing temperature it is expected that electrons located at high energies will dominate the transport mechanism, and cause the barrier to become higher. The very high value of the ideality factor at low temperatures is related to the tunneling current domination, however with increasing temperature the thermionic transport mechanism dominates [59].

Capacitance-voltage measurements were performed at room temperature with a frequency of 1 MHz for both samples and are presented in the Fig. 7(a). As NiO is fully depleted at zero bias, the plot of $1/C^2$ vs V shown in Fig. 7(b) can be used to estimate the donor concentration (N_d) in Ga_2O_3 . The straight line for both diodes indicates that the doping profiles are homogeneous. The N_d was found to be $2\times 10^{17}~\text{cm}^{-3}$ and $1.4\times 10^{16}~\text{cm}^{-3}$ for the fresh and annealed samples, respectively. The annealed sample exhibits lower value of free carrier concentration as compared with the fresh sample. The high N_d in the fresh sample could be due to surface contamination or Si surface congregation occurred during the epitaxial growth.

4.2. DLTS and Laplace (DLTS) measurements

DLTS technique has been used to investigate the effects of post growth annealing on electrically active defects in Ga_2O_3 or near the Ga_2O_3/NiO interface [60]. The experimental DLTS parameters used were: a reverse bias, $V_R=-2$ V, a filling pulse height, $V_P=0$ V, a filling pulse time, $t_P=1$ msec, and a rate window of 500 s⁻¹. Fig. 8 illustrates a typical DLTS spectrum for both samples. In fresh sample, three negative peaks are detected in the temperature range 100 K - 400 K, which corre-

spond to three electron traps labeled as E_1 , E_2 and E_3 . After annealing, it is clear from Fig. 8 that the post-growth annealing process reduces the number of traps to only one electron trap E_3 .

To resolve the broad DLTS peaks, Laplace DLTS (LDLTS) measurements [61] were carried out. The activation energies of these traps were determined from Arrhenius plots as shown in Fig. 9. A summary of these trap parameters, including the activation energy, the trap concentrations, and the capture cross-section, is presented in Table 2.

As shown in Fig. 9, the donor trap E₁ with an activation energy 0.10 ± 0.01 eV and concentration 5.5×10^{17} cm⁻³ observed in β -Ga₂O₃ is likely to be the same trap detected by Neal et al. [28]. Using temperature dependent Hall-effect measurements up to 1000 K and admittance spectroscopy (AS) technique, they suggested that the presence of this center is most likely related to a native defect, such as an anti-site or interstitial [28]. It is also possible that silicon on octahedrally coordinated Ga(II) of Ga₂O₃ could be responsible for the 110 meV donor [28]. However, this trap was annihilated after annealing process. The trap E_2 with activation energy 0.15 \pm 0.02 eV and trap concentrations of 9.4×10^{16} cm⁻³, was observed in the fresh sample. A similar deep defect was detected in pulsed-laser-deposited epitaxial films of β-Ga₂O₃ using thermally stimulated current [62]. This trap was also detected using AS technique in β -(Al $_{0.14}$ Ga $_{0.86}$) $_2$ O $_3$ /Ga $_2$ O $_3$ heterojunctions. It was suggested that E2 could be due to trapping/detrapping of electrons by Sn donors in the substrate and the energy required to overcome the potential barrier between β -(Al $_{0.14}$ Ga $_{0.86}$) $_2$ O $_3$ ternary and the Ga₂O₃ substrate, respectively [63]. The traps E₃ was detected in both samples (fresh and annealed) with activation energy ranging from 0.16 eV to 0.19 eV. This defect level was detected in both ZCO/Ga2O3 and NiO/Ga2O3 heterojunctions with activation energies ranging from 0.18 to 0.23 eV using Thermal Admittance Spectroscopy (TAS) [53]. This defect level with similar activation energy was also found in homoepitaxial β -Ga₂O₃ thin films fabricated by metal organic chemical vapor deposition or by plasma enhanced molecular beam epitaxy [64,65]. This defect was also observed in Ga2O3 films grown by halide vapor phase epitaxy on p-type diamond substrates [66], and in Ge-doped (010) β -Ga2O3 layers grown by plasma-assisted molecular beam epitaxy using DLTS technique and suggested this trap may be related to double donor Ge dopants [65]. This may indicate that this defect is common in epitaxial β -Ga₂O₃ thin films [53]. Furthermore, the results demonstrated that the RTA process reduce the concentration of E_3 trap from 2×10^{17} cm⁻³ to $4.3 \times 10^{14}~\text{cm}^{-3}$, while E_1 and E_2 traps were annihilated. In the fresh sample, the electron traps E1 and E3 are also revealed by DLTS at -4 V (see Figure S2) but with lower concentrations as compared to the bias condition of -2 V, indicating that both E_1 and E_3 are bulk traps in the Si-doped β -Ga $_2$ O $_3$ epitaxial layer. This is in contrast to trap E $_2$ which was observed only at a reverse bias of -2 V while it was absent at -4 V suggesting that it is probably an interface trap. For the annealed sample, the electron trap E3 is also revealed but with higher concentration.

5. Modeling

TCAD of SILVACO was used to model the HJD with the aim of correlating trap dynamics to device characteristics. TCAD solves the basic drift-diffusion semiconductor equations, Poisson and continuity equations and include thermionic tunneling above and through the heterojunction, respectively [67–69].

Poisson equation is given by [67-69]:

$$div(\varepsilon \nabla \psi) = -q \left(p - n + N_D^+ - N_A^- \pm N_t^{\pm} \right) \tag{3}$$

where, ψ is the electrostatic potential, ε is the permittivity, p and n are free holes and electrons concentrations, respectively, $N_D^+(N_A^-)$ is the ionized donor (acceptor) density and N_t^\pm is the ionized traps density. For NiO and Ga₂O₃, $N_A^- = \frac{N_A}{1+\frac{1}{2}\exp(\frac{E_f-E_d}{KT})}$ and $N_d^+ = \frac{N_d}{1+\frac{1}{2}\exp(\frac{E_d-E_f}{KT})}$ the activation energies for each layer presented in Table 3.

Table 2 Traps parameters for both device at $V_R = -2 \; V, \, V_P = 0 \; V,$ and $t_P = 1 \; msec.$

Sample	Trap	Activation energy(eV)	Trap concentration(cm ⁻³)	Capture cross-section (cm ²)
Fresh	E ₁	0.10 ± 0.01	5.5 × 10 ¹⁷	4 × 10 ⁻²⁰
	E_2	0.15 ± 0.02	9.4×10^{16}	3×10^{-20}
	E_3	0.18 ± 0.01	2×10^{17}	9.1×10^{-21}
Annealed	E_3	0.17 ± 0.01	4.3×10^{14}	5.2×10^{-21}

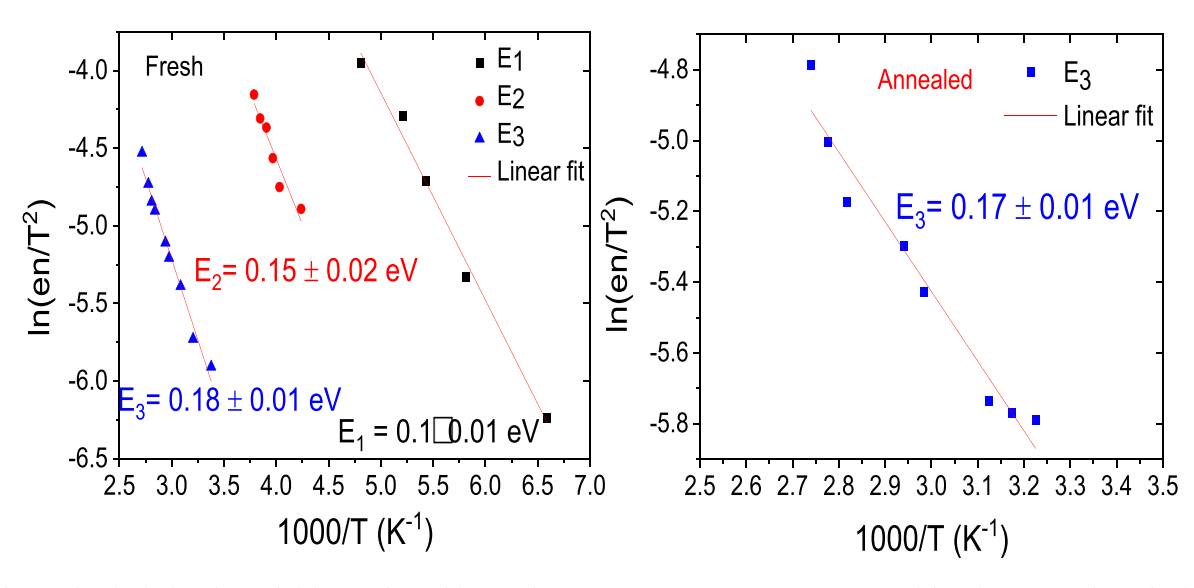


Fig. 9. Arrhenius plots for fresh and annealed devices obtained from Laplace DLTS at $V_R = -2$ V. (For interpretation of the references to color in this figure legend, the reader is referred to the web version of this article.)

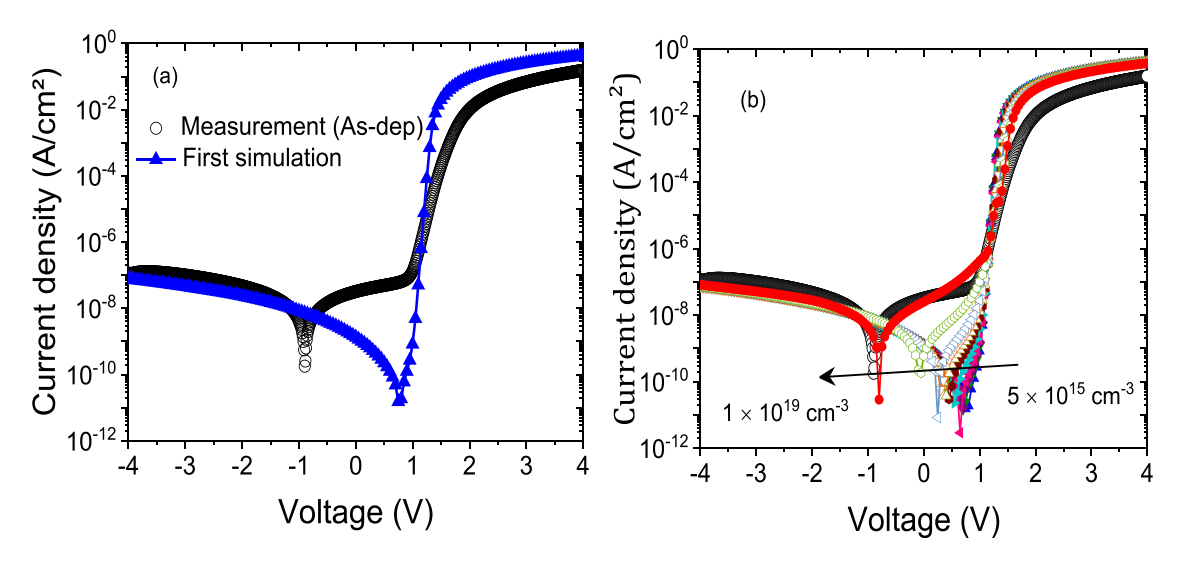


Fig. 10. The simulated FHJ J-V characteristics for: (a) homogeneous NiO density $(5 \times 10^{16} \text{ cm}^{-3})$ and (b) inhomogeneous variable NiO surface acceptor density. (For interpretation of the references to color in this figure legend, the reader is referred to the web version of this article.)

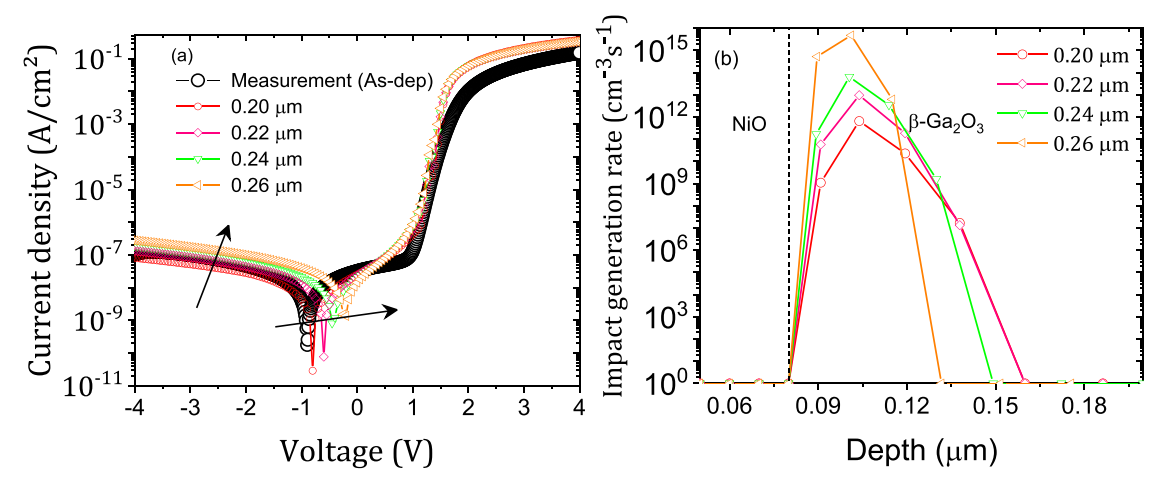


Fig. 11. Effect of the E₂ trap location depth on (a) the simulated J-V characteristics and (b) impact generation rate at equilibrium. (For interpretation of the references to color in this figure legend, the reader is referred to the web version of this article.)

Table 3 Properties of each layer of the studied NiO/ β -Ga₂O₃ HJD.

Parameters	Sn: β -Ga $_2$ O $_3$ [67,70,71]	Si: β -Ga ₂ O ₃ [28,67,70]	NiO[72-74]
Thickness (μm)	600	10	0.1
Bandgap (eV)	4.8	4.8	3.71
Affinity (eV)	4	4	1.46
Hole mobility (cm ² V ⁻¹ s ⁻¹)	10	10	1
Electron mobility (cm ² V ⁻¹ s ⁻¹)	172	300	12
Doping density (N _a and N _d) (cm ⁻³)	1×10^{18} (n-type)	$1.4 \times 10^{16} - 2 \times 10^{17}$ (n-type)	$5 \times 10^{15} - 1 \times 10^{19}$ (p-type)
Ionization energy (eV)	E _c -0.21	E _c -0.11	$E_{v} + 0.26$
Relative permittivity	12.6	11	10.7
N_c (cm ⁻³)	3.7×10^{18}	3.7×10^{18}	2.8×10^{19}
N_v (cm ⁻³)	5×10^{18}	5×10^{18}	1.1×10^{19}
Minority carrier lifetime (ns)	0.21	0.21	260

The continuity equations; for electrons and holes; defined in steady states are given by [67–69]:

$$0 = \frac{1}{a}div\overrightarrow{J_n} + G_n - R_n \tag{4}$$

$$0 = -\frac{1}{a}div\overrightarrow{J_p} + G_p - R_p \tag{5}$$

where, G_n and G_p are the generation rates for electrons and holes, R_n and R_p are the recombination rate for electrons and holes. \vec{J}_n and \vec{J}_p are the electron and hole current density which are given in term of quasi-Fermi level $(\phi_n$ and $\phi_p)$ and mobility $(\mu_n$ and $\mu_p)$ as [67–69]:

$$\vec{J}_n = -q\mu_n n \nabla \phi_n \tag{6}$$

$$\vec{J}_p = -q\mu_p p \nabla \phi_p \tag{7}$$

Traps are represented by their ionized density N_t^\pm . The sign \pm depends on whether the trap is a majority or a minority carrier so that $N_t^+ = f N_t$ and $N_t^- = (1-f)N_t$, f is the occupancy function given by $f = \frac{\sigma_n n + \sigma_p p}{\sigma_n (n + n_t) + \sigma_p (p + p_t)}$, $\sigma_n(p)$ is the trap capture cross-section for electrons (holes). Furthermore, the recombination rate is related to traps through the well-known Shockley-Read-Hall recombination (SRH) formula $R_{n,p} = \frac{pn - n_t^2}{\tau_{0n}(p + p_t) + \tau_{0p}(n + n_t)}$ with $n_t = n_t exp(-(E_t - E_t)/kT)$ and $p_t = n_t exp(-(E_t - E_t)/kT)$, τ_{0n} and τ_{0p} are the minority carrier lifetime which are also related to traps through $\tau_{0n(p)} = \frac{1}{v_{thn(p)}\sigma_{n(p)}N_t}$ where $v_{thn(p)}$ is the thermal velocity of electrons (holes).

In addition, thermionic emission Eq. (1) and ((2)) and tunneling currents are taken into account since they might be present in heterojunctions.

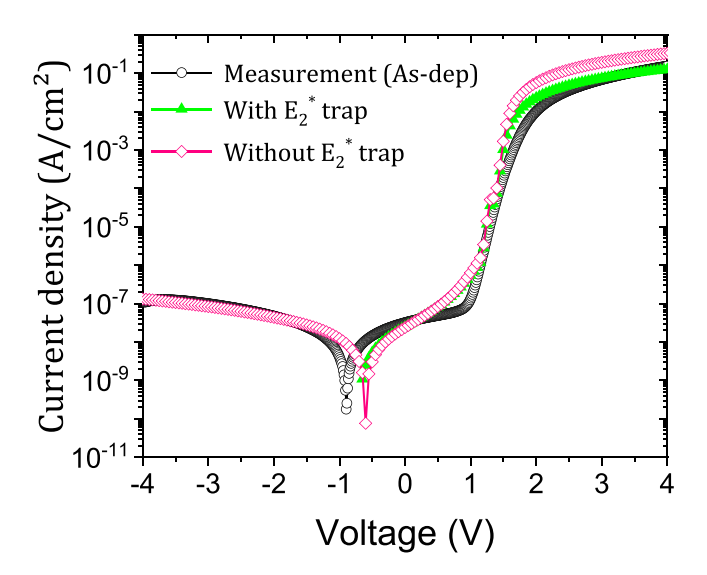


Fig. 12. Effect of E_c -0.75 trap on J-V characteristics. (For interpretation of the references to color in this figure legend, the reader is referred to the web version of this article.)

The tunneling current is given by [75]:

$$J_{T} = \frac{A^{*}T_{L}}{K_{B}} \int_{\epsilon}^{\infty} \Gamma(E') \ln\left(\frac{1 + F_{s}(E')}{1 + F_{m}(E')}\right) dE'$$
(8)

where A^* , T_L , K_B , ϵ , $F_s(E')$ and $F_m(E')$ are effective Richardson's coefficient (41.11 $Acm^{-2}K^{-2}$), lattice temperature, Boltzmann constant,

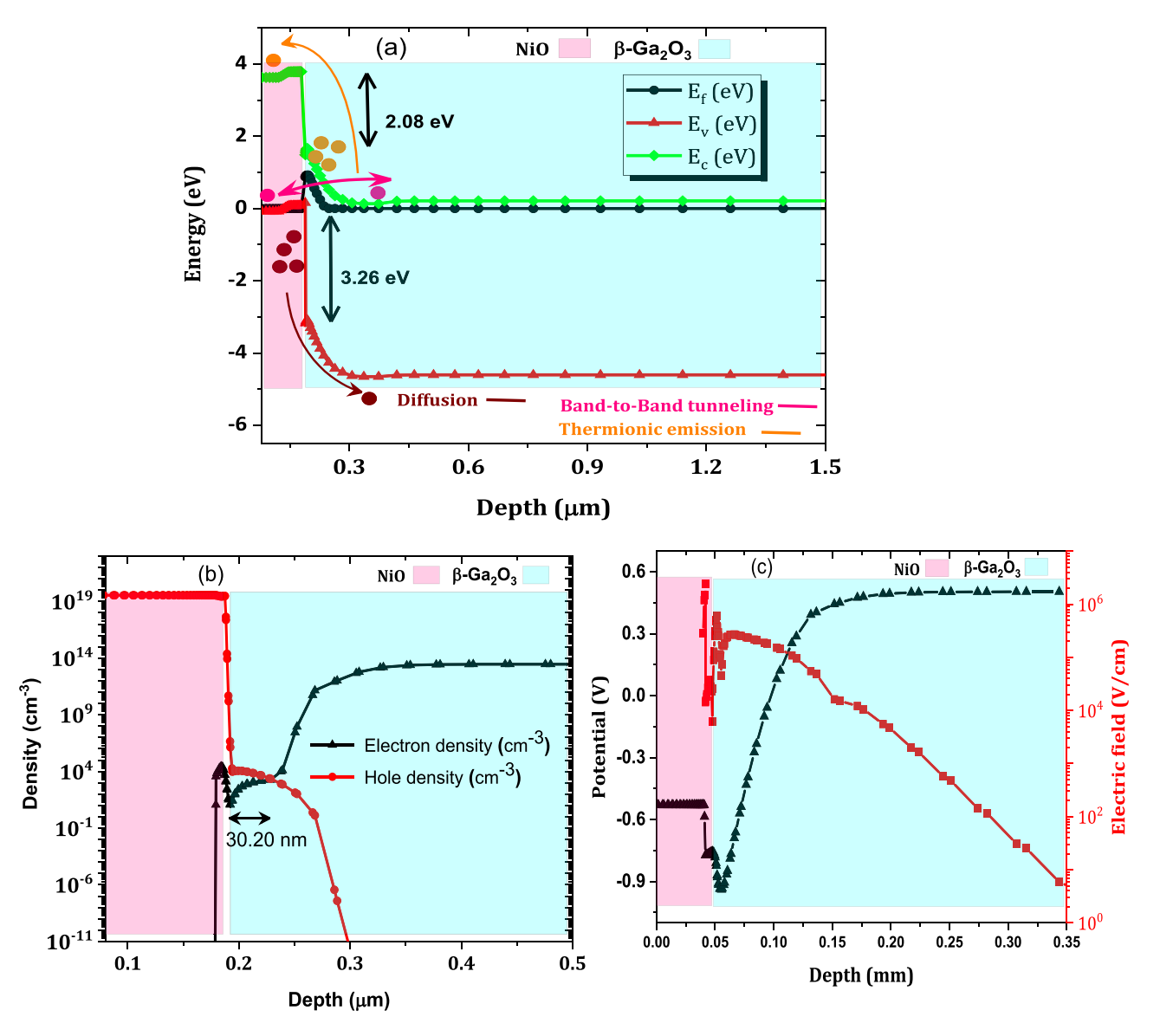


Fig. 13. Equilibrium (0 V) band diagram and transport mechanisms (a), free carriers' profile (b), and potential and electric field profile (c). (For interpretation of the references to color in this figure legend, the reader is referred to the web version of this article.)

electrons energy, and Maxwell- Boltzmann distribution in the semiconductor and metal, respectively, and $\Gamma(E')$ is the tunneling probability given by [75]:

$$\Gamma(\epsilon) = \exp\left[-2\frac{\sqrt{2m^*}}{\hbar} \int_{x_1}^{x_2} \sqrt{E_c(x) - \epsilon} dx\right]$$
 (9)

Here, $E_c(x)$ and (x_1, x_2) are the potential energy distribution of Schottky barrier diode and classical turning points, respectively.

Furthermore, for mobilities dependent concentration and temperature are considered using analytic model at each layer which is given by [76]:

$$\mu_n(T, N_d) = \mu_{minn} \left(\frac{T}{300}\right)^{n1} + \frac{\mu_{maxn} \left(\frac{T}{300}\right)^{m1} - \mu_{minn} \left(\frac{T}{300}\right)^{n1}}{1 + \left(\frac{T}{300}\right)^{\alpha1} \left(\frac{N_d}{N_{d0}}\right)^{\gamma1}}$$
(10)

$$\mu_{p}(T, N_{a}) = \mu_{minp} \left(\frac{T}{300}\right)^{n2} + \frac{\mu_{maxp} \left(\frac{T}{300}\right)^{m2} - \mu_{minp} \left(\frac{T}{300}\right)^{n2}}{1 + \left(\frac{T}{300}\right)^{\alpha2} \left(\frac{N_{a}}{N_{oft}}\right)^{\gamma2}}$$
(11)

Where μ_{minn} , μ_{minp} , μ_{maxn} , μ_{maxp} , n1, m1, $\alpha1$, $\gamma1$, N_{d0} , n2, m2, $\alpha2$, N_{a0} and $\gamma2$ are fitting parameters presented in Table S2 for majority carriers at each layer and Figure S3 shows the used NiO hole mobility dependant acceptor density.

In addition to SRH, Auger recombination and mobility dependent electric field are considered in this simulation.

5.1. Modeling NiO/ β -Ga $_2$ O $_3$ heterojunction

In this section, fresh and annealed NiO/ β -Ga₂O₃ heterojunction characteristics were modeled in order to understand conduction mechanisms as well as deep levels effects. The starting modeling parameters of each layer of the heterojunction are shown in Table 3. The difference between fresh and annealed samples is in their deep levels content.

5.2. Fresh NiO/ β -Ga₂O₃ heterojunction (FHJ)

In FHJ, the electron traps E_1 and E_3 are revealed by DLTS at -2 V (Fig. 9) and -4 V (Figure S2) pulse heights, which indicates that both E_1 and E_3 are bulk traps which are considered in epitaxial layer (Si-doped β -Ga₂O₃) in contrast to E_2 , which was seen at -2 V while it was absent

at -4 V indicating that it is probably an interface trap. The depletion region width for the -2 and -4 V reverse biases is roughly estimated to be 0.204 and 0.232 µm, respectively, for the effective doping density of 2×10^{17} cm³ estimated from C-V characteristics. The 0.204 and 0.232 µm depletion region widths are initially considered the location limits of the interface and bulk traps, respectively. The NA in the p-type NiO is first assumed to be $8 \times 10^{16} \text{ cm}^{-3}$. The simulated J-V characteristics compared to measurements are presented in Fig. 10(a). The disagreement between simulation and measurement, especially the voltage position of the J-V curve peak, may be related to several reasons. The first possible reason could be due to the inhomogeneity of NiO acceptor density. For example Lee el al [77]. have extracted Ni and oxygen profiles using energy dispersive X-ray spectroscopy (EDS) and they found that Ni and oxygen have an inhomogeneity profiles, this will effect on the acceptor density profile. We will, therefore, study the effect of NiO surface acceptor density. This parameter is scanned from 5×10^{15} to $1 \times 10^{19} \ \text{cm}^{-3}$ and the obtained J-V characteristics, compared to measurements, is presented in Fig. 10(b).

The voltage position of the J-V curve peak is the most affected region. As the NiO surface acceptor density increases the peaks of the simulated and the measured currents get closer. This behavior is related to the increase in the band-to-band tunneling current [78]. A good agreement is achieved for a surface acceptor density of $1\times10^{19}~{\rm cm}^{-3}$.

The second plausible explanation is the $\rm E_2$ trap location depth. Initially this interface trap is assumed to be located in the region between the interface and 0.204 µm (the depletion region limit corresponding to -2 V). This trap location may well be beyond this position. This probable limit is varied between 0.20 and 0.26 µm and the corresponding J-V characteristics are presented in Fig. 11(a). With increasing trap depth, the leakage current increased. This may be related to the increase in NiO/ β -Ga₂O₃ interface generation of free carriers from this trap level as shown in Fig. 11(b). A good agreement at reverse voltage was obtained for a depth of about 0.220 µm which is less than 0.234 µm (corresponding to -4 V). This may well be the reason that the $\rm E_2$ trap was absent in DLTS at -4 V.

The series resistance region is not affected by the E_2 trap location depth. Therefore, a further investigation is required. The E_2^* trap ($E_c^{-0.75}$) is one of the most observed traps in β -Ga₂O₃ [32,79,80] at a density of 10^{13} – 10^{14} cm⁻³. This trap is not observed in this study perhaps because of the fact that it is usually observed in bulk β -Ga₂O₃ and affects the forward current [32]. Therefore, this trap is considered in Sn-doped β -Ga₂O₃ substrate with density 4.1×10^{13} cm⁻³ [32] and the modeling-measurement difference is reduced as presented in Fig. 12.

Now, after obtaining a fairly good agreement, the equilibrium band diagram, free carriers' profiles, electric field and potential profiles are extracted and are shown in Fig. 13. A type-II NiO/ β -Ga₂O₃ heterojunction as shown in Fig. 13(a) was obtained which is in agreement with [26,32]. In this work, three transport mechanisms are present: thermionic emission, diffusion and band-to-band tunneling as detailed in Fig. 13(a). Free holes diffuse from NiO to the surface of β -Ga₂O₃ with a diffusion length of about \sim 30.20 nm as shown in Fig. 13(b). Then, because of high NiO hole density, band-to-band tunneling plays an important role while the thermionic emission mechanism finds a suitable barrier to overcome.

From the free carrier profile, the equilibrium depletion spreads mainly in β -Ga₂O₃ because of high NiO surface acceptor density and its width is $\sim 0.182~\mu m$ which is obtained from the equilibrium potential profile (Fig. 13(c)). Furthermore, the built-in potential value (V_{bi}) extracted from the equilibrium potential profile is about 1.30 V, which is different from the turn-on voltage (V_{on}) of about 1.40 V for fresh HJ sample extracted from the simulated J-V characteristics shown in Fig. 12. This small deviation of 0.1 V between the two values may be related to the effect of the considered interfacial traps. A high equilibrium electric field with unusual profile at the NiO/ β -Ga₂O₃ interface may be due to hole diffusion and the considered surface (Fig. 13(c)).

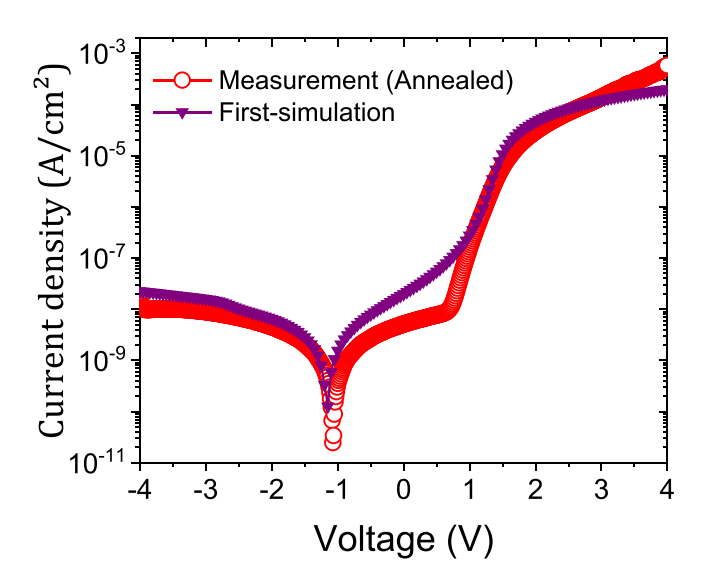


Fig. 14. The simulated J-V characteristics compared to measurement for AHJ. (For interpretation of the references to color in this figure legend, the reader is referred to the web version of this article.)

5.2.1. Annealed NiO/ β -Ga₂O₃ heterojunction (AHJ)

When the sample was annealed, only one trap was revealed by DLTS, namely E₃. The activation energy of this trap is E_c-0.17 eV and its density is $4.3 \times 10^{14}~\text{cm}^{-3}$ at -2~V but increased to $3.1 \times 10^{16}~\text{cm}^{-3}$ at -4 V. This indicates that this trap has a non-uniform profile. Therefore, the AHJ was modeled using the same established parameters for the FHJ except for the traps, NiO acceptor density, and the donor density in the Si-doped β -Ga₂O₃. Consequently, a simple presentation of the trap profile was proposed. This profile consists of two regions with different densities. The first starts from the interface and has a depth equal to the depletion region limit at −2 V (0.685 µm for the AHJ) with a density of $4.3 \times 10^{14} \text{cm}^{-3}$. The second started from 0.685 μm to the rest of the active region (Si-doped β -Ga₂O₃) of the sample with a density of 3.1 ×10¹⁶ cm⁻³. Furthermore, we have found that after annealing the sheet resistance increased from $3.99 \times 10^7 \,\Omega/\text{cm}^2$ to $1.47 \times 10^8 \,\Omega/\text{cm}^2$, indicating that the free hole density decreased after annealing. The extracted hole density from sheet resistance with the consideration of the proposed hole mobility model was about $2.35 \times 10^{15}~\text{cm}^{-3}$ (N_A = $6 \times 10^{16}~\text{cm}^{-3}$ because the free hole density is just 4.7% of N_A). The N_A value is very close to the measured value of 6×10^{16} cm⁻³. This decrease of hole density may be related to the decrease in oxygen vacancy in NiO layer. In addition, the donor density of the considered Si-doped β-Ga₂O₃ layer is $1.4\times10^{16}\ \text{cm}^{-3}.$ The simulated J-V curves show good agreement with the experimental results as illustrated in Fig. 14.

6. Conclusion

The effect of RTA on the electrical and optical properties of NiO/ β -Ga₂O₃ heterojunction diodes have been investigated using Capacitance-Voltage, Current-Voltage, DLTS, Laplace DLTS, Photoluminescence, micro-Raman spectroscopy techniques, and SILVACO-TCAD numerical simulator. The heterojunction diode is designed to make NiO fully depleted at zero bias, thus allowing for study of the properties of β -Ga₂O₃ and its interface with NiO. We found that the annealed samples showed better diode performance. This was in agreement with the optical results which demonstrated an enhancement in the photoluminescence peak intensity after RTA. This enhancement is explained by a rise in the density of gallium vacancies. In addition, the RTA resulted in an improvement of the electrical characteristics of the devices and a reduction of the number of electrically active traps. SILVACO TCAD was used to model different effects. Values of the E₂ trap depth from the β -Ga₂O₃ surface and the NiO surface hole density were determined, enabling a good agreement

with experimental results for fresh and annealed samples. Furthermore, because of the high NiO surface hole density, we have demonstrated that band-to-band tunneling transport mechanism is dominant. Applying the RTA process on NiO/ β -Ga₂O₃ heterojunction diodes resulted in superior optical and electrical properties than those of the fresh samples, which are required for potential applications in next generation power devices. The demonstrated NiO/ β -Ga₂O₃ heterojunction can be open a route toward future bipolar devices such as heterojunction gate field-effect-transistors (HJ-FETs) or normally-off FET [81,82].

Authors Contributions

All authors contributed equally to this work.

Declaration of Competing Interest

The authors declare that they have no known competing financial interests or personal relationships that could have appeared to influence the work reported in this paper.

Data availability

Data will be made available on request.

Acknowledgements

Abdulaziz Almalki would like to acknowledge support from Taibah University-Yanbu for providing scholarship for his PhD degree. This work was supported by "Fundação de Amparo à Pesquisa do Estado de São Paulo (grant numbers 2019/23488-5 and 19/07442-5), "Conselho Nacional de Desenvolvimento Científico e Tecnológico" (CNPq) and "Financiadora de Estudos e Projetos" (FINEP) (grant number 01.22.0178.00 - MATSemBGL (14796)), the U.S. National Science Foundation under Grants ECCS-2100504 and ECCS-2230412, and the Center for Power Electronics Systems Industry Consortium.

Supplementary materials

Supplementary material associated with this article can be found, in the online version, at doi:10.1016/j.mtelec.2023.100042.

References

- [1] J.A. Spencer, A.L. Mock, A.G. Jacobs, M. Schubert, Y. Zhang, M.J. Tadjer, A review of band structure and material properties of transparent conducting and semiconducting oxides: Ga₂O₃, Al2O3, In₂O₃, ZnO, SnO₂, CdO, NiO, CuO, and Sc2O3, Appl. Phys. Rev. 9 (2022) 11315, doi:10.1063/5.0078037.
- [2] S.J. Pearton, F. Ren, M. Tadjer, J. Kim, Perspective: Ga₂O₃ for ultra-high power rectifiers and MOSFETS, J. Appl. Phys. 124 (2018) 220901, doi:10.1063/1.5062841.
- [3] M. Higashiwaki, K. Sasaki, A. Kuramata, T. Masui, S. Yamakoshi, Gallium oxide (Ga2O3) metal-semiconductor field-effect transistors on single-crystal β-Ga₂O₃ (010) substrates, Appl. Phys. Lett. 100 (2012) 13504, doi:10.1063/1.3674287.
- [4] Y. Wang, H. Gong, Y. Lv, X. Fu, S. Dun, T. Han, H. Liu, X. Zhou, S. Liang, J. Ye, R. Zhang, A. Bu, S. Cai, Z. Feng, 2.41 kV vertical P-Nio/n-Ga₂O₃ heterojunction diodes with a record Baliga's figure-of-merit of 5.18 GW/cm², IEEE Trans. Power Electron. 37 (2022) 3743–3746, doi:10.1109/TPEL.2021.3123940.
- [5] Y. Zhang, T. Palacios, (Ultra)wide-bandgap vertical power FinFETs, IEEE Trans. Electron Devices 67 (2020) 3960–3971, doi:10.1109/TED.2020.3002880.
- [6] B. Wang, M. Xiao, X. Yan, H.Y. Wong, J. Ma, K. Sasaki, H. Wang, Y. Zhang, High-voltage vertical $\rm Ga_2O_3$ power rectifiers operational at high temperatures up to 600 K, Appl. Phys. Lett. 115 (2019) 263503, doi:10.1063/1.5132818.
- [7] M. Xiao, B. Wang, J. Liu, R. Zhang, Z. Zhang, C. Ding, S. Lu, K. Sasaki, G.-Q. Lu, C. Buttay, Y. Zhang, Packaged Ga₂O₃ Schottky rectifiers with over 60-A surge current capability, IEEE Trans. Power Electron. 36 (2021) 8565–8569, doi:10.1109/TPEL.2021.3049966.
- [8] B. Wang, M. Xiao, J. Knoll, C. Buttay, K. Sasaki, G.-Q. Lu, C. Dimarino, Y. Zhang, Low thermal resistance (0.5 K/W) Ga₂O₃ Schottky rectifiers with double-side packaging, IEEE Electron. Device Lett. 42 (2021) 1132–1135, doi:10.1109/LED.2021.3089035.
- [9] W. Li, K. Nomoto, Z. Hu, D. Jena, H.G. Xing, Field-plated Ga₂O₃ trench Schottky barrier diodes with a BV2/Ron,sp of up to 0.95 GW/cm2, IEEE Electron. Device Lett. 41 (2020) 107–110, doi:10.1109/LED.2019.2953559.
- [10] N. Allen, M. Xiao, X. Yan, K. Sasaki, M.J. Tadjer, J. Ma, R. Zhang, H. Wang, Y. Zhang, Vertical Ga₂O₃ Schottky barrier diodes with small-angle beveled field plates: a Baliga's figure-of-merit of 0.6 GW/cm², IEEE Electron Device Lett. 40 (2019) 1399– 1402. doi:10.1109/LED.2019.2931697.

- [11] Y. Wang, Y. Lv, S. Long, X. Zhou, X. Song, S. Liang, T. Han, X. Tan, Z. Feng, S. Cai, M. Liu, High-voltage (201) β -Ga₂O₃ vertical Schottky barrier diode with thermally-oxidized termination, IEEE Electron Device Lett. 41 (2020) 131–134, doi:10.1109/LED.2019.2956016.
- [12] C.-H. Lin, Y. Yuda, M.H. Wong, M. Sato, N. Takekawa, K. Konishi, T. Watahiki, M. Yamamuka, H. Murakami, Y. Kumagai, M. Higashiwaki, Vertical Ga₂O₃ Schottky barrier diodes with guard ring formed by nitrogen-ion implantation, IEEE Electron Device Lett. 40 (2019) 1487–1490, doi:10.1109/LED.2019.2927790.
- [13] H. Zhou, Q. Yan, J. Zhang, Y. Lv, Z. Liu, Y. Zhang, K. Dang, P. Dong, Z. Feng, Q. Feng, J. Ning, C. Zhang, P. Ma, Y. Hao, High-performance vertical β-Ga₂O₃ Schottky barrier diode with implanted edge termination, IEEE Electron Device Lett. 40 (2019) 1788–1791. doi:10.1109/LED.2019.2939788.
- [14] C. Ma, Z. Wu, Z. Jiang, Y. Chen, W. Ruan, H. Zhang, H. Zhu, G. Zhang, J. Kang, T.-Y. Zhang, J. Chu, Z. Fang, Exploring the feasibility and conduction mechanisms of P-type nitrogen-doped β-Ga₂O₃ with high hole mobility, J. Mater. Chem. C. 10 (2022) 6673–6681, doi:10.1039/D1TC05324H.
- [15] Z.Y. Wu, Z.X. Jiang, C.C. Ma, W. Ruan, Y. Chen, H. Zhang, G.Q. Zhang, Z.L. Fang, J.Y. Kang, T.-Y. Zhang, Energy-driven multi-step structural phase transition mechanism to achieve high-quality p-type nitrogen-doped β-Ga₂O₃ films, Mater. Today Phys. 17 (2021) 100356, doi:10.1016/j.mtphys.2021.100356.
- [16] Z.X. Jiang, Z.Y. Wu, C.C. Ma, J.N. Deng, H. Zhang, Y. Xu, J.D. Ye, Z.L. Fang, G.Q. Zhang, J.Y. Kang, T.-Y. Zhang, P-type β -Ga $_2$ O $_3$ metal-semiconductor-metal solar-blind photodetectors with extremely high responsivity and gain-bandwidth product, Mater. Today Phys. 14 (2020) 100226, doi:10.1016/j.mtphys.2020.100226.
- [17] X. Zhou, M. Li, J. Zhang, L. Shang, K. Jiang, Y. Li, L. Zhu, Z. Hu, J. Chu, High quality P-type Mg-doped β -Ga₂O₃– δ films for solar-blind photodetectors, IEEE Electron Device Lett. 43 (2022) 580–583, doi:10.1109/LED.2022.3151476.
- [18] A. Kyrtsos, M. Matsubara, E. Bellotti, On the feasibility of p-type Ga $_2$ O $_3,$ Appl. Phys. Lett. 112 (2018) 032108, doi:10.1063/1.5009423.
- [19] H.H. Gong, X.H. Chen, Y. Xu, F.-F. Ren, S.L. Gu, J.D. Ye, A 1.86-kV double-layered NiO/ β -Ga $_2$ O $_3$ vertical p–n heterojunction diode, Appl. Phys. Lett. 117 (2020) 022104, doi:10.1063/5.0010052.
- [20] F. Zhou, H. Gong, W. Xu, X. Yu, Y. Xu, Y. Yang, F. Ren, S. Gu, Y. Zheng, R. Zhang, J. Ye, H. Lu, 1.95-kV Beveled-mesa ${\rm NiO}/\beta$ -Ga $_2{\rm O}_3$ heterojunction diode with 98.5% conversion efficiency and over million-times overvoltage ruggedness, IEEE Trans. Power Electron 37 (2022) 1223–1227, doi:10.1109/TPEL.2021.3108780.
- [21] X. Lu, X. Zhou, H. Jiang, K.W. Ng, Z. Chen, Y. Pei, K.M. Lau, G. Wang, 1-kV sputtered p-NiO/n-Ga₂O₃ heterojunction diodes with an ultra-low leakage current below 1 μA/cm2, IEEE Electron Device Lett. 41 (2020) 449–452, doi:10.1109/LED.2020.2967418.
- [22] Y. Kokubun, S. Kubo, S. Nakagomi, All-oxide p-n heterojunction diodes comprising p-type NiO and n-type β-Ga₂O₃, Appl. Phys. Express 9 (2016) 91101, doi:10.7567/apex.9.091101.
- [23] T. Watahiki, Y. Yuda, A. Furukawa, M. Yamamuka, Y. Takiguchi, S. Miyajima, Heterojunction p- $\text{Cu}_2\text{O}/\text{n-}\text{Ga}_2\text{O}_3$ diode with high breakdown voltage, Appl. Phys. Lett. 111 (2017) 222104, doi:10.1063/1.4998311.
- [24] J.C. Gallagher, A.D. Koehler, M.J. Tadjer, N.A. Mahadik, T.J. Anderson, S. Budhathoki, K.-M. Law, A.J. Hauser, K.D. Hobart, F.J. Kub, Demonstration of CuI as a P-N heterojunction toβ-Ga₂O₃, Appl. Phys. Express. 12 (2019) 104005, doi:10.7567/1882-0786/ab420e.
- [25] F. Wu, Y. Wang, G. Jian, G. Xu, X. Zhou, W. Guo, J. Du, Q. Liu, S. Dun, Z. Yu, Y. Lv, Z. Feng, S. Cai, S. Long, Superior performance β-Ga₂O₃ junction barrier Schottky diodes implementing p-NiO heterojunction and beveled field plate for hybrid Cockcroft–Walton voltage multiplier, IEEE Trans. Electron Devices 70 (2023) 1199–1205. doi:10.1109/TED.2023.3239062.
- [26] H. Gong, X. Chen, Y. Xu, Y. Chen, F. Ren, B. Liu, S. Gu, R. Zhang, J. Ye, Band alignment and interface recombination in NiO/β -Ga₂ O ₃ Type-II p-n heterojunctions, IEEE Trans. Electron Devices 67 (2020) 3341–3347, doi:10.1109/TED.2020.3001249.
- [27] H.H. Gong, X.X. Yu, Y. Xu, X.H. Chen, Y. Kuang, Y.J. Lv, Y. Yang, F.-F. Ren, Z.H. Feng, S.L. Gu, Y.D. Zheng, R. Zhang, J.D. Ye, β -Ga₂O₃ vertical heterojunction barrier Schottky diodes terminated with p-NiO field limiting rings, Appl. Phys. Lett. 118 (2021) 202102, doi:10.1063/5.0050919.
- [28] A.T. Neal, S. Mou, R. Lopez, J.V. Li, D.B. Thomson, K.D. Chabak, G.H. Jessen, Incomplete ionization of a 110 meV unintentional donor in β-Ga₂O₃ and its effect on power devices, Sci. Rep. 7 (2017) 13218, doi:10.1038/s41598-017-13656-x.
- [29] Z. Zhang, E. Farzana, A.R. Arehart, S.A. Ringel, Deep level defects throughout the bandgap of (010) β -Ga $_2$ O $_3$ detected by optically and thermally stimulated defect spectroscopy, Appl. Phys. Lett. 108 (2016) 052105, doi:10.1063/1.4941429.
- [30] R. Sun, Y.K. Ooi, A. Bhattacharyya, M. Saleh, S. Krishnamoorthy, K.G. Lynn, M.A. Scarpulla, Defect states and their electric field-enhanced electron thermal emission in heavily Zr-doped β -Ga $_2$ O $_3$ crystals, Appl. Phys. Lett. 117 (2020) 212104, doi:10.1063/5.0029442.
- [31] J. Montes, C. Kopas, H. Chen, X. Huang, T. Yang, K. Fu, C. Yang, J. Zhou, X. Qi, H. Fu, Y. Zhao, Deep level transient spectroscopy investigation of ultra-wide bandgap (201) and (001) β -Ga $_2$ O $_3$, J. Appl. Phys. 128 (2020) 205701, doi:10.1063/5. 0021859.
- [32] Z. Wang, H. Gong, C. Meng, X. Yu, X. Sun, C. Zhang, X. Ji, F. Ren, S. Gu, Y. Zheng, R. Zhang, J. Ye, Majority and minority carrier traps in NiO/β-Ga 2 O 3 p + -n heterojunction diode, IEEE Trans. Electron Devices 69 (2022) 981–987, doi:10.1109/TED.2022.3143491.
- [33] D. Ködderitzsch, W. Hergert, Z. Szotek, W.M. Temmerman, Vacancy-induced half-metallicity in MnO and NiO, Phys. Rev. B. 68 (2003) 125114, doi:10.1103/Phys-RevB.68.125114.

- [34] B. Wang, M. Xiao, J. Spencer, Y. Qin, K. Sasaki, M.J. Tadjer, Y. Zhang, 2.5 kV vertical Ga₂O₃ Schottky rectifier with graded junction termination extension, IEEE Electron Device Lett. 44 (2023) 221–224, doi:10.1109/LED.2022.3229222.
- [35] B.M. Janzen, P. Mazzolini, R. Gillen, A. Falkenstein, M. Martin, H. Tornatzky, J. Maultzsch, O. Bierwagen, M.R. Wagner, Isotopic study of Raman active phonon modes in β-Ga₂O₃, J. Mater. Chem. C. 9 (2021) 2311–2320, doi:10.1039/D0TC04101G.
- [36] C. Kranert, C. Sturm, R. Schmidt-Grund, M. Grundmann, Raman tensor elements of β -Ga₂O₃, Sci. Rep. 6 (2016) 35964, doi:10.1038/srep35964.
- [37] T. Onuma, S. Fujioka, T. Yamaguchi, Y. Itoh, M. Higashiwaki, K. Sasaki, T. Masui, T. Honda, Polarized Raman spectra in β -Ga₂O₃ single crystals, J. Cryst. Growth 401 (2014) 330–333, doi:10.1016/j.jcrysgro.2013.12.061.
- [38] B. Liu, M. Gu, X. Liu, Lattice dynamical, dielectric, and thermodynamic properties of β-Ga₂O₃ from first principles, Appl. Phys. Lett. 91 (2007) 172102, doi:10.1063/1.2800792.
- [39] D. Machon, P.F. McMillan, B. Xu, J. Dong, High-pressure study of the β -to- α transition in Ga₂O₃, Phys. Rev. B. 73 (2006) 94125, doi:10.1103/PhysRevB.73.094125.
- [40] D. Dohy, G. Lucazeau, A. Revcolevschi, Raman spectra and valence force field of single-crystalline β Ga₂O₃, J. Solid State Chem. 45 (1982) 180–192, doi:10.1016/0022-4596(82)90274-2.
- [41] D. Dohy, G. Lucazeau, Valence force field and raman spectra of β Ga₂O₃, J. Mol. Struct. 79 (1982) 419–422, doi:10.1016/0022-2860(82)85094-1.
- [42] Q.D. Ho, T. Frauenheim, P. Deák, Origin of photoluminescence in β -Ga₂O₃, Phys. Rev. B. 97 (2018) 115163, doi:10.1103/PhysRevB.97.115163.
- [43] M.D. McCluskey, Point defects in Ga₂O₃, J. Appl. Phys. 127 (2020) 101101, doi:10.1063/1.5142195.
- [44] J. Hao, M. Cocivera, Optical and luminescent properties of undoped and rare-earth-doped Ga_2O_3 thin films deposited by spray pyrolysis, J. Phys. D. Appl. Phys. 35 (2002) 433–438, doi:10.1088/0022-3727/35/5/304.
- [45] D. Guo, Q. Guo, Z. Chen, Z. Wu, P. Li, W. Tang, Review of Ga_2O_3 -based optoelectronic devices, Mater. Today Phys. 11 (2019) 100157, doi:10.1016/j.mtphys.2019.100157.
- [46] R. Tian, M. Pan, Q. Sai, L. Zhang, H. Qi, H.F. Mohamed, Crucial role of oxygen vacancies in scintillation and optical properties of undoped and Al-doped β -Ga₂O₃ single crystals, Crystals (2022) 12, doi:10.3390/cryst12030429.
- [47] E.G. Víllora, M. Yamaga, T. Inoue, S. Yabasi, Y. Masui, T. Sugawara, T. Fukuda, Optical spectroscopy study on β-Ga₂O₃, Jpn. J. Appl. Phys. 41 (2002) L622, doi:10.1143/JJAP.41.L622.
- [48] W. Hao, Q. He, K. Zhou, G. Xu, W. Xiong, X. Zhou, G. Jian, C. Chen, X. Zhao, S. Long, Low defect density and small I V curve hysteresis in NiO/β -Ga 2 O₃ pn diode with a high PFOM of 0.65 GW/cm 2, Appl. Phys. Lett. 118 (2021) 043501, doi:10.1063/5.0038349.
- [49] Z. Rebaoui, W. Bachir Bouiajra, M. Abboun Abid, A. Saidane, D. Jammel, M. Henini, J.F. Felix, SiC polytypes and doping nature effects on electrical properties of ZnO-SiC Schottky diodes, Microelectron. Eng. 171 (2017) 11–19, doi:10.1016/j.mee.2017.01.010.
- [50] K. Horio, H. Yanai, Numerical modeling of heterojunctions including the thermionic emission mechanism at the heterojunction interface, IEEE Trans. Electron Devices 37 (1990) 1093–1098, doi:10.1109/16.52447.
- [51] S.M. Sze, K.K. Ng, Metal-semiconductor contacts, Phys. Semicond. Devices (2006) 134–196, doi:10.1002/9780470068328.ch3.
- [52] J.H. Werner, Schottky barrier and pn-junctionI/V plots Small signal evaluation, Appl. Phys. A Solids Surf. 47 (1988) 291–300, doi:10.1007/BF00615935.
- [53] P. Schlupp, D. Splith, H. von Wenckstern, M. Grundmann, Electrical properties of vertical p-NiO/n-Ga 2 O 3 and p-ZnCo 2 O 4 /n-Ga 2 O 3 pn-heterodiodes, Phys. Status Solidi Appl. Mater. Sci. 216 (2019) 1–6, doi:10.1002/pssa.201800729.
- [54] S.M. Sze, K.K. Ng, Physics of Semiconductor Devices, 3rd ed., John wiley & Sons, Hoboken, NJ, USA, 2006.
- [55] M. Grundmann, R. Karsthof, H. von Wenckstern, Interface recombination current in Type II heterostructure bipolar diodes, ACS Appl. Mater. Interfaces 6 (2014) 14785– 14789. doi:10.1021/am504454g.
- [56] G. Jian, Q. He, W. Mu, B. Fu, H. Dong, Y. Qin, Y. Zhang, H. Xue, S. Long, Z. Jia, H. Lv, Q. Liu, X. Tao, M. Liu, Characterization of the inhomogeneous barrier distribution in a Pt/(100) β -Ga ₂ O ₃ Schottky diode via its temperature-dependent electrical properties, AIP Adv. 8 (2018) 015316, doi:10.1063/1.5007197.
- [57] T. Zhang, Y. Shen, Q. Feng, X. Tian, Y. Cai, Z. Hu, G. Yan, Z. Feng, Y. Zhang, J. Ning, Y. Xu, X. Lian, X. Sun, C. Zhang, H. Zhou, J. Zhang, Y. Hao, The investigation of hybrid PEDOT:PSS/β-Ga₂O₃ deep ultraviolet Schottky barrier photodetectors, Nanoscale Res. Lett. 15 (2020) 163, doi:10.1186/s11671-020-03397-8.
- [58] H. Sheoran, B.R. Tak, N. Manikanthababu, R. Singh, Temperature-dependent electrical characteristics of Ni/Au vertical Schottky barrier diodes on β-Ga₂O₃ epilayers, ECS J. Solid State Sci. Technol. 9 (2020) 55004, doi:10.1149/2162-8777/ab96ad.
- [59] M. Labed, J.H. Park, A. Meftah, N. Sengouga, J.Y. Hong, Y.-K. Jung, Y.S. Rim, Low temperature modeling of Ni/ β -Ga $_2$ O $_3$ Schottky barrier diode interface, ACS Appl. Electron. Mater. 3 (2021) 3667–3673, doi:10.1021/acsaelm.1c00647.
- [60] D.V. Lang, Deep-level transient spectroscopy: a new method to characterize traps in semiconductors, J. Appl. Phys. 45 (1974) 3023–3032, doi:10.1063/1.1663719.

- [61] L. Dobaczewski, A.R. Peaker, K.B. Nielsen, Laplace-transform deep-level spectroscopy: the technique and its applications to the study of point defects in semi-conductors, J. Appl. Phys. 96 (2004) 4689–4728, doi:10.1063/1.1794897.
- [62] B. Wang, D. Look, K. Leedy, Deep level defects in β -Ga $_2$ O $_3$ pulsed laser deposited thin films and Czochralski-grown bulk single crystals by thermally stimulated techniques, J. Appl. Phys. 125 (2019) 105103, doi:10.1063/1.5049820.
- [63] A.Y. Polyakov, N.B. Smirnov, I.V. Schemerov, A.V. Chernykh, E.B. Yakimov, A.I. Kochkova, J. Yang, C. Fares, F. Ren, S.J. Pearton, Deep traps and persistent photocapacitance in β -(Al $_{0.14}$ Ga $_{0.86}$) $_2$ O $_3$ /Ga $_2$ O $_3$ heterojunctions, J. Appl. Phys. 125 (2019) 095702, doi:10.1063/1.5080941.
- [64] A.Y. Polyakov, N.B. Smirnov, I.V. Shchemerov, D. Gogova, S.A. Tarelkin, S.J. Pearton, Compensation and persistent photocapacitance in homoepitaxial Sndoped β -Ga $_2$ O $_3$, J. Appl. Phys. 123 (2018) 115702, doi:10.1063/1.5025916.
- [65] E. Farzana, E. Ahmadi, J.S. Speck, A.R. Arehart, S.A. Ringel, Deep level defects in Ge-doped (010) β -Ga $_2$ O $_3$ layers grown by plasma-assisted molecular beam epitaxy, J. Appl. Phys. 123 (2018) 161410, doi:10.1063/1.5010608.
- [66] A.Y. Polyakov, V.I. Nikolaev, S.A. Tarelkin, A.I. Pechnikov, S.I. Stepanov, A.E. Nikolaev, I.V. Shchemerov, E.B. Yakimov, N.V. Luparev, M.S. Kuznetsov, A.A. Vasilev, A.I. Kochkova, M.I. Voronova, M.P. Scheglov, J. Kim, S.J. Pearton, Electrical properties and deep trap spectra in Ga₂ O₃ films grown by halide vapor phase epitaxy on p-type diamond substrates, J. Appl. Phys. 129 (2021) 185701, doi:10.1063/5.0044531.
- [67] M. Labed, N. Sengouga, M. Labed, A. Meftah, S. Kyoung, H. Kim, Y.S. Rim, Modeling a Ni $/\beta$ -Ga $_2$ O $_3$ Schottky barrier diode deposited by confined magnetic-field-based sputtering, J. Phys. D. Appl. Phys. 54 (2021) 115102, doi:10.1088/1361-6463/abce2c.
- [68] M. Labed, N. Sengouga, M. Labed, A. Meftah, S. Kyoung, H. Kim, Y.S. Rim, Modeling and analyzing temperature-dependent parameters of Ni/β-Ga₂O₃ Schottky barrier diode deposited by confined magnetic field-based sputtering, Semicond. Sci. Technol. 36 (2021) 35020, doi:10.1088/1361-6641/abe059.
- [69] M. Labed, N. Sengouga, A. Meftah, A. Meftah, Y.S. Rim, Study on the improvement of the open-circuit voltage of NiOx/Si heterojunction solar cell, Opt. Mater. (Amst). 120 (2021) 111453, doi:10.1016/j.optmat.2021.111453.
- [70] J. Lee, E. Flitsiyan, L. Chernyak, J. Yang, F. Ren, S.J. Pearton, B. Meyler, Y.J. Salzman, Effect of 1.5 MeV electron irradiation on β -Ga $_2$ O $_3$ carrier lifetime and diffusion length, Appl. Phys. Lett. 112 (2018) 082104, doi:10.1063/1.5011971.
- [71] A.Y. Polyakov, N.B. Smirnov, I.V. Shchemerov, D. Gogova, S.A. Tarelkin, S.J. Pearton, Compensation and persistent photocapacitance in homoepitaxial Sndoped β-Ga₂O₃, J. Appl. Phys. 123 (2018) 115702, doi:10.1063/1.5025916.
- [72] D. Attafi, A. Meftah, R. Boumaraf, M. Labed, N. Sengouga, Enhancement of silicon solar cell performance by introducing selected defects in the SiO₂ passivation layer, Optik (Stuttg.) 229 (2021) 166206, doi:10.1016/j.ijleo.2020.166206.
- [73] S. Thamri, M.H. Raouadi, H. Ezzaouia, Study of the performance of a ZnO-NiO/Si nanocomposite-based solar cell, ECS J. Solid State Sci. Technol. 9 (2020) 125005, doi:10.1149/2162-8777/abd378.
- [74] W.B. Zhang, N. Yu, W.Y. Yu, B.Y. Tang, Stability and magnetism of vacancy in NiO: a GGA+U study, Eur. Phys. J. B. 64 (2008) 153–158, doi:10.1140/epjb/e2008-00303-x.
- [75] M. Labed, N. Sengouga, A. Meftah, M. Labed, S. Kyoung, H. Kim, Y.S. Rim, Leakage current modelling and optimization of β-Ga₂ O₃ Schottky barrier diode with Ni contact under high reverse voltage, ECS J. Solid State Sci. Technol. 9 (2020) 125001, doi:10.1149/2162-8777/abc834.
- [76] M.-W. Ha, O. Seok, H. Lee, H.H. Lee, Mobility models based on forward current-voltage characteristics of P-type pseudo-vertical diamond Schottky barrier diodes, Micromachines (Basel) 11 (2020), doi:10.3390/mi11060598.
- [77] Y.H. Lee, H. Song, K.-H. Kim, J. Oh, Investigation of surface reactions in metal oxide on Si for efficient heterojunction Si solar cells, APL Mater. 7 (2019) 071106, doi:10.1063/1.5100884.
- [78] S. Gundapaneni, M. Bajaj, R.K. Pandey, K.V.R.M. Murali, S. Ganguly, A. Kottan-tharayil, Effect of band-to-band tunneling on junctionless transistors, IEEE Trans. Electron Devices 59 (2012) 1023–1029, doi:10.1109/TED.2012.2185800.
- [79] A.Y. Polyakov, I.-H. Lee, N.B. Smirnov, E.B. Yakimov, I.V. Shchemerov, A.V. Chernykh, A.I. Kochkova, A.A. Vasilev, P.H. Carey, F. Ren, D.J. Smith, S.J. Pearton, Defects at the surface of β-Ga₂ O₃ produced by Ar plasma exposure, APL Mater. 7 (2019) 061102, doi:10.1063/1.5109025.
- [80] Z. Galazka, β -Ga $_2$ O $_3$ for wide-bandgap electronics and optoelectronics, Semicond. Sci. Technol. 33 (2018) 113001, doi:10.1088/1361-6641/aadf78.
- [81] X. Zhou, Q. Liu, W. Hao, G. Xu, S. Long, Normally-off β-Ga₂O₃ power heterojunction field-effect-transistor realized by p-NiO and recessed-gate, in: Proc. Int. Symp. Power Semicond. Devices ICs. 2022-May, 2022, pp. 101–104, doi:10.1109/ISPSD49238.2022.9813678.
- [82] C. Wang, H. Gong, W. Lei, Y. Cai, Z. Hu, S. Xu, Z. Liu, Q. Feng, H. Zhou, J. Ye, J. Zhang, R. Zhang, Y. Hao, Demonstration of the p-NiOx/n-Ga₂O₃ heterojunction gate FETs and diodes with BV2/Ron,sp Figures of merit of 0.39 GW/cm2 and 1.38 GW/cm2, IEEE Electron Device Lett. 42 (2021) 485–488, doi:10.1109/LED.2021.3062851.